New Dion−Jacobson-Type Layered Perovskite Oxyfluorides, $ASrNb_2O_6F$ (A = Li, Na, and Rb)

Jin-Ho Choy,* Jong-Young Kim, Seung-Joo Kim, and Joon-Sung Sohn

National Nanohybrid Materials Laboratory, School of Chemistry and Molecular Engineering, College of Natural Sciences, Seoul National University, Seoul 151-747, Korea

Oc Hee Han

Korea Basic Science Institute, 52 Yeoeun-dong Yusung-Gu, Taejon 305-333, Korea

Received August 21, 2000. Revised Manuscript Received December 4, 2000

New Dion−Jacobson-type layered perovskite oxyfluorides, $ASrNb_2O_6F$ (A = Li, Na, and Rb), have been prepared by conventional solid-state reaction, and their fluorine distribution in an anion sublattice was studied by performing ^{19}F MAS NMR spectroscopic analyses and lattice energy calculations to probe the evolution of interlayer cationic conductivitiy upon fluorine substitution. From these comparative studies, it is found that the fluorine anions are randomly distributed in two distinct crystallographic sites among three possible sites in the oxyfluoride lattice, that is, the equatorial site of NbO_6 octahedra ($O_{equatorial}$) and the central site of two corner-sharing NbO_6 octahedra along the *c* axis (O_{center}). On the other hand, the substituted fluorine does not prefer to occupy the O_{apex} site, which interacts ionically with an alkali metal cation (A^+) in the interlayer, because the ($Nb-O_{apex}$) bond is too strongly covalent to be replaced by the ionic Nb−F bond. We have also compared systematically the Li and Na ion conductivities for the oxyfluorides, $ASrNb_2O_6F$, with those for the corresponding oxides, $ALaNb_2O_7$ (A = Li and Na), and found that the fluorination of the perovskite layer gives rise to an enhancement of ionic transport in the interlayer space.

Introduction

Recently, considerable research efforts have focused on Ruddlesden−Popper-type perovskite-related oxides, $A_2[A'_{n-1}B_nO_{3n+1}]$, and Dion−Jacobson-type ones, $A[A'_{n-1}B_nO_{3n+1}]$ (A, A′ = alkaline or alkaline-earth metal, B = transition metal), because they possess some unique physicochemical properties such as Brönsted acidity,[1] photocatalytic activity,[2] ionic conductivity,[3] and intercalation behavior.[4] More recently, it was reported that cation-deficient $La_{2/3-x}Li_{3x}TiO_3$ perovskite exhibits excellent ionic conductivity of ca. 10^{-3} S cm^{-1} at room temperature,[5a−f] which gives an impetus to prepare a new lithium ionic conductor such as $LiSr_{1.65}\square_{0.35}M_{1.3}M'_{1.7}O_9$ (M = Ti and Zr; M′ = Nb and Ta) through aliovalent substitution for perovskite oxides.[5g−h] In addition to such compounds, new ionic-conducting Ruddlesden−Popper phases such as $Li_4Sr_3Nb_{5.77}Fe_{0.23}O_{19.77}$, $Li_4Sr_3Nb_6O_{20}$,[5i] $A_2Ln_2Ti_3O_{10}$ (A = K, Na; Ln = Lanthanides),[5j] and $NaLnTiO_4$[5k] were also prepared. Even though a lot of studies were carried out for cation-modified perovskites, few attempts have been made to modify the anionic components in these compounds. In this regard, we have attempted to prepare new ion-conducting Dion−Jacobson-type oxyfluorides of $ASrNb_2O_6F$ (A = Li, Na, and Rb) not only to explore new ionic conductors but also to investigate the effect of fluorine incorporation on ionic conductivity of layered oxide.

In Dion−Jacobson-type layered perovskite oxides, perovskite blocks (corner-sharing BO_6 octahedra) are interstratified with alkali metal cation (A^+) layers in a 1:1 fashion. As shown in Figure 1b, the $A-O_{apex}$ bond, competing with the $Nb-O_{apex}$ bond, is significantly weaker than the $Nb-O_{apex}$ bond. It is, therefore, expected that an enhanced Nb−O(apex) bond strength might provide an effective pathway for two-dimensional conduction. In this respect, an attempt has been made to reduce the $A-O_{apex}$ bond strength by the substitution

* To whom all correspondences should be addressed. Fax: +82-2-872-9864. Tel.: +82−2−880−6658. E-mail: jhchoy@plaza.snu.ac.kr.

(1) Gopalakrishnan, J.; Uma, S.; Bhat, V. *Chem. Mater.* **1993**, *5*, 132.

(2) (a) Domen, K.; Yoshimura, J.; Sekine, T.; Tanaka A.; Onishi, T. *Catal. Lett.* **1990**, *4*, 339. (b) Yoshimura, J.; Ebina, Y.; Kondo, J.; Domen, K.; Tanaka A. *J. Phys. Chem.* **1993**, *97*, 1970.

(3) (a) Sato, M.; Watanabe, J.; Uematsu, K. *J. Solid State Chem.* **1993**, *107*, 460. (b) Byeon, S. H.; Park, K. *J. Solid State Chem.* **1996**, *121*, 430. (c) Sato, M.; Abo, J.; Jin, T. *Solid State Ionics* **1992**, *57*, 285.

(4) (a) Jacobson, A. J.; Johnson, J. W.; Lewandowski, J. T. *Inorg. Chem.* **1985**, *24*, 3729. (b) Uma, S.; Gopalakrishnan, J. *J. Solid State Chem.* **1993**, *102*, 332. (c) Mohan Ram, R. A.; Clearfield, A. *J. Solid State Chem.* **1991**, *94*, 45.

(5) (a) Inaguma, Y.; Liquan, C.; Itoh, M.; Nakamura, T.; Uchida, T.; Ikuta, H.; Wakihara, M. *Solid State Commun.* **1993**, *86*, 689. (b) Kawai, H.; Kuwano, J. *J. Electrochem. Soc.* **1994**, *141*, L78. (c) Varez, A.; Garcia-Alvarado, F.; Moran, E.; Alario-Franco, M. A. *J. Solid State Chem.* **1995**, *118*, 78. (d) Fourquet, J. L.; Duroy, H.; Crosnier-Lopez, M. P. *J. Solid State Chem.* **1996**, *127*, 283. (e) Bohnke, O.; Bohnke, C.; Fourquet, J. L. *Solid State Ionics* **1996**, *91*, 21. (f) Alonzo, J. A.; Sanz, J.; Santamaria, J.; Carlos, L.; Varez, A.; Fernadez-Diaz, M. T. *Angew. Chem. Int. Ed.* **2000**, *39*, 619. (g) Robertson, A. D.; Garcia Martin, S.; Coats, A.; West, A. R. *J. Mater. Chem.* **1995**, *5*, 1405. (h) Thangadurai, V.; Shakula, A. K.; Gopalakrishnan, J. *Chem. Mater.* **1999**, *11*, 835. (i) Bhuvanesh, N. S. P.; Crosnier-Lopez, M. P.; Bohnke, O.; Emery, J.; Fourquet, J. L. *Chem. Mater.* **1999**, *11*, 643. (j) Gopalakrishnan, J.; Bhat, V. *Inorg. Chem.* **1987**, *26*, 4299. (k) Byeon, S. H.; Park, K.; Itoh, M. *J. Solid State Chem.* **1996**, *121*, 430.

10.1021/cm000673g CCC: $20.00
Published on Web 02/10/2001

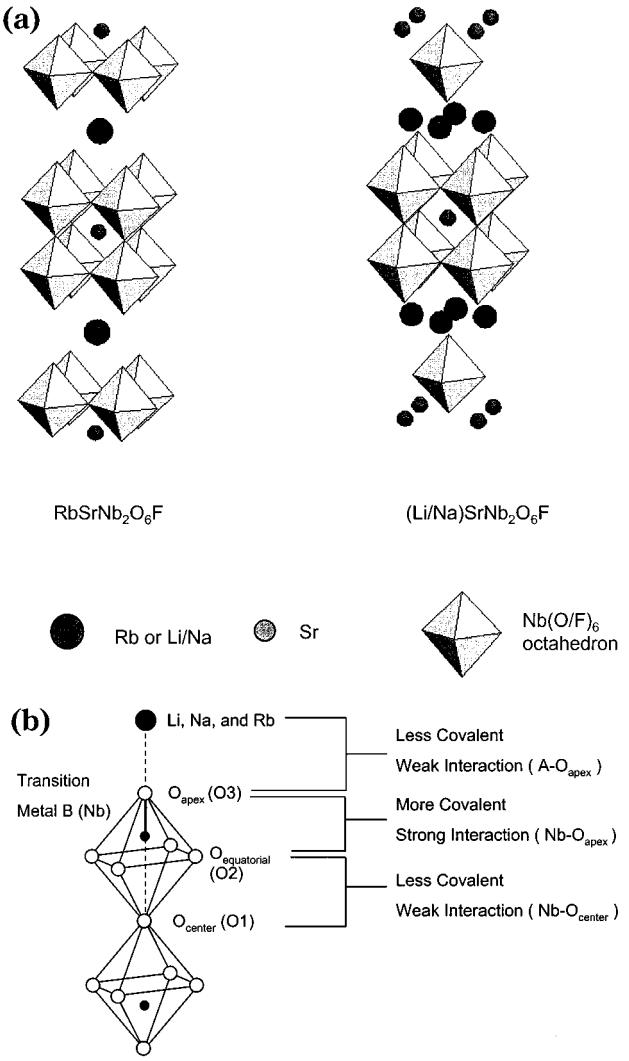

Figure 1. (a) Crystal structures of $ASrNb_2O_6F$ (A = Na and Li) and $RbSrNb_2O_6F$ (b) local structure around niobium in the present system.

of fluorine for oxygen to improve ionic mobility. The substituted fluorine will be mainly populated at the $O_{center/equatorial}$ sites because the $Nb-O_{apex}$ bond is too strongly covalent to be replaced by the ionic Nb−F bond. The formation of the $Nb-F_{center/equatorial}$ bonds with more ionic character reinforces the $Nb-O_{apex}$ bond, which should compete with the $Nb-O_{center}$ and $Nb-O_{equatorial}$ bonds by pathways of 180° and 90°, respectively.[6] An increased $Nb-O_{apex}$ bond covalency gives rise to the weakening of the $A-O_{apex}$ bond strength, which results in an increase of alkali metal ion mobility.

Considering intimate correlation between ionic conductivity and chemical bonding nature, the specification of a fluorine anion arrangement in the oxyfluoride lattice is of primary importance. In the Ruddlesden−Popper-type oxyfluorides such as $Sr_2CuO_2F_{2+\delta}$,[7] Ba_2InO_3F, and $Ba_3In_2O_5F_2$,[8a−b] it was found that oxide and fluoride ions are ordered, which leads to a new superstructure. In contrast, some oxyfluorides such as ScOF,[8c] ThOF,[8d] and $CdNdTi_2O_6F$[8e] exhibit disordered arrangements of fluoride and oxide. In such cases, it is not possible to determine the fluorine position by conventional X-ray and neutron diffraction methods because of their similar atomic scattering factors and ionic radii. For this reason, we have applied ^{19}F MAS NMR spectroscopy to the present system to substantiate spatial distribution of fluorine anions, complementarily to lattice energy calculation. Techniques for high resolution MAS NMR spectra of spin 1/2-nuclei in solids are now well developed and provide site-specific information about site populations, chemical bonding, and molecular structure.[9−13] On the basis of the fluorine position determined by ^{19}F MAS NMR and lattice energy calculation, the influence of fluorine substitution on ionic conductivity was discussed from the viewpoint of competing bond principle. Such information on the relationship between the local chemical environment and ionic conductivity will be quite important in designing new ionic-conducting materials by controlling the chemical bonding nature.

Experimental Section

Sample Preparation. The polycrystalline $RbSrNb_2O_6F$ compound was prepared by solid-state reaction between $SrNb_2O_6$ and RbF. The precursor $SrNb_2O_6$ was obtained by firing the stoichiometric quantities of high-purity $SrCO_3$ and Nb_2O_5 at 1000 °C for 2 days. Then, $SrNb_2O_6$ was well mixed with RbF, pelletized in a glovebox, and heated at 750 °C in a sealed gold tube filled with highly purified N_2 gas. The product was washed thoroughly with distilled water and dried at 250 °C in an ambient atmosphere for 1 day. The ion exchange reaction was performed for 3 days by adding the well-ground $RbSrNb_2O_6F$ powder to a $LiNO_3$ molten salt at 300 °C for $LiSrNb_2O_6F$ and to a $NaNO_3$ one at 350 °C for $NaSrNb_2O_6F$, respectively. During the ion exchange reaction, the mother solution was refreshed every day. Finally, the products were washed with distilled water and dried at 250 °C for 1 day.

Powder X-ray Diffraction. Powder XRD patterns were recorded using a Philips PW 3710 diffractometer in the range $2\theta = 20°-100°$ in a step scan mode with counts for 5 s at a 0.02° interval. Detailed crystallographic parameters were derived from Rietveld refinement using the RIETAN-94 program.[14]

^{19}F NMR Analysis. ^{19}F MAS (magic angle spinning) NMR spectra were obtained using the DSX 400 spectrometer (Bruker Analytik GmbH, Germany) equipped with a CP/MAS probe for 4-mm rotors. A Larmor frequency of 376.4 MHz, a spectral width of 500 kHz corresponding to 1 μs dwell time, and an acquisition time of 4.15 or 5.00 ms were employed. And the spinning rate, pulse repetition delay, and pulse length were chosen to be 3−15 kHz, 1 s, and 1 μs corresponding to a 30° flip angle, respectively. The acquisition number for a spectrum was varied between 340 and 2048. The chemical shift of 1 N

(6) (a) Goodenough, J. B. *Prog. Solid State Chem*. **1971**, *5*, 145. (b) Ming, Z. L.; Demazeau, G.; Pouchard, M.; Dance, J. M.; Hagenmuller, P. *J. Solid State Chem*. **1989**, *78*, 46.

(7) Al-Mamouri, M.; Edwards, P. P.; Greaves, C.; Slaski, M. *Nature* **1994**, *369*, 382.

(8) (a) Needs, R. L.; Weller, M. T. *J. Chem. Soc., Dalton Trans.* **1995,** 3015. (b) Needs, R. L.; Weller, M. T. *J. Chem. Soc. Chem. Commun.* **1995**, 353. (c) Vlasse, M.; Saux, M.; Echegut, P.; Villeneuve, G. *Mater. Res. Bull.* **1979**, *14*, 807. (d) Rannou, J.-P.; Lucas, J. *Mater. Res. Bull.* **1996**, *4*, 443. (e) Grannec, J.; Baudry, H.; Ravez, J.; Portier, J. *J. Solid State Chem.* **1974**, *10*, 66.

(9) Stejskal, E. O.; Memory, J. D. *High-Resolution NMR in the Solid State*; Oxford University Press: New York, 1994.

(10) Ernst, R. R.; Bodenhausen, G.; Wokaun, A. *Principles of Nuclear Magnetic Resonance in One and Two Dimensions*; Oxford University Press: Oxford, 1987.

(11) Diehl, P.; Fluck, E.; Gunther, H.; Kosfeld, R. *NMR Basic Principles and Progress*; Spinger-Verlag: Berlin, 1994; Vols. 30−33.

(12) Griffiths, J.; Griffin, R. G. *Anal. Chim. Acta* **1993**, *283*, 1081.

(13) Garbow, J. R.; Gullion, T. In *Carbon-13 NMR Spectroscopy of Biological systems*; Beckmann, N., Ed.; Academic Press: San Diego, 1995; Chapter 3.

(14) Izumi, F. In *Rietveld Method*; Young, R. A., Ed.; Oxford University Press: Oxford, 1993; Chapter 13.

Table 1. Quantitative Chemical Analysis for Fluorine and Alkali Metals (A) in $ASrNb_2O_6F$ (A = Li, Na, and Rb)

	$LiSrNb_2O_6F$	$NaSrNb_2O_6F$	$RbSrNb_2O_6F$
F	0.98(7)	1.06(4)	0.97(4)
alkali metal	0.92(7)	1.12(11)	0.91(5)

aqueous $LiAsF_6$ solution was referenced as −69.5 ppm.[15,16] ^{19}F MAS NMR spectra for all the compounds were fitted with a Bruker-Winfit program with Gaussian and Lorentzian line shapes. The spectra at various spinning rates were simulated to obtain chemical shift parameters such as isotropic chemical shift (δ_i), asymmetry parameter (η), and anisotropy ($\Delta\delta$). Although ^{19}F homonuclear and heteronuclear couplings between ^{19}F and the other atoms can influence the line broadening, according to theoretical calculation, the full width at half-maximum (fwhm) due to the dipolar line broadening in static spectra is only 3.6 kHz at most, whereas the experimental spectra have signals covering more than 90 kHz. Therefore, the present F NMR spectra are mainly affected by chemical shift anisotropy interaction rather than by dipolar interaction. The population in each site was calculated by a line integral.

Ionic Conductivity Measurement. Ionic conductivities were measured by a complex impedance technique between 5 Hz and 13 MHz using a Hewlett-Packard 4192A LF impedance analyzer in a temperature range of 200−400 °C. The specimens were prepared as follows: the powder samples were dehydrated by heating at 250 °C for 4 h and then pelletized under 400 MPa, and the gold electrodes on two opposite sides of the disk were deposited by an evaporation technique.

Chemical Analysis. To determine the contents of alkali metal ions, atomic absorption spectroscopic analyses were performed with a Perkin-Elmer 3100 spectrometer (Table 1). $NaSrNb_2O_6F$, $KSrNb_2O_6F$, and $RbSrNb_2O_6F$ were dissolved as follows: The solids were melted with an excess amount of $LiBO_2$ at 850 °C for 5 min. And then, the melts were dissolved in $HCl + H_2O_2/H_2O$ immediately. For $LiSrNb_2O_6F$, the melt was dissolved in $HCl + H_2O_2 + HF/H_2O$ in a Teflon beaker. Quantitative chemical analysis for fluorine was carried out by ^{19}F-MAS NMR with the spinning rates of 5 and 13 kHz.[15,16] The integrated peak area was compared with the number of fluorine atoms using BaF_2 as a reference (Table 1).

Results and Discussion

Crystallographic Analysis. The crystal structures for $RbSrNb_2O_6F$ and $Li(Na)SrNb_2O_6F$ are analogous to those for $RbLaNb_2O_7$ and $Li(Na)LaNb_2O_7$, respectively.[17−19] All the peaks in the XRD pattern of $RbSrNb_2O_6F$ (Figure 2a) can be successfully indexed on the basis of tetragonal symmetry, indicating the formation of a single phase. The [001] zone axis electron diffraction (see Supporting information) and XRD patterns exhibit no reflection conditions, suggesting the $P4/***$ type space groups ($P4$, $P\bar{4}$, $P4/m$, $P422$, $P4mm$, $P\bar{4}2m$, $P4m2$, and $P4/mmm$).[20,21] Among these space groups, the structural refinement with $P4/mmm$ only gives physically meaningful crystallographic parameters. As listed in Table 2, $RbSrNb_2O_6F$ has the unit-cell parameters of $a = 3.8503(1)$ Å and $c = 11.2841(3)$ Å with the space group of $P4/mmm$. The calculated

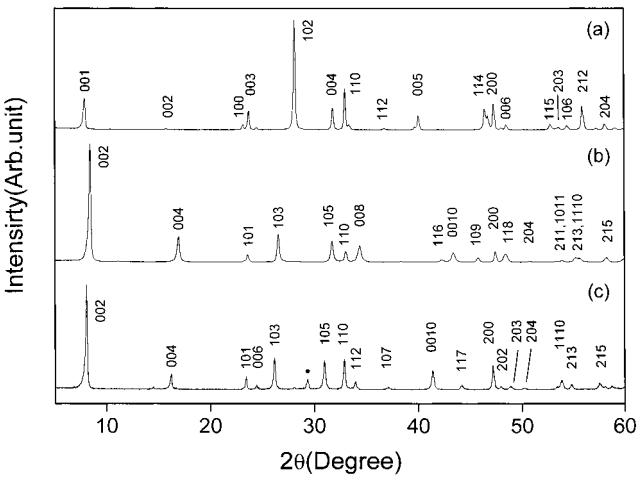

Figure 2. X-ray diffraction patterns for (a) $RbSrNb_2O_6F$, (b) $LiSrNb_2O_6F$, and (c) $NaSrNb_2O_6F$. In (c), circle indicates the impurity of the pyrochlore phase.

Table 2. Crystallographic Data for $RbSrNb_2O_6F$ and $LiSrNb_2O_6F$

	compound	
	$RbSrNb_2O_6F$	$LiSrNb_2O_6F$
space group	$P4/mmm$	$I4/mmm$
a (Å)	3.8503(1)	3.8304(2)
c (Å)	11.2841(3)	20.837(1)
unit cell volume (Å^3)	167.3	305.7
calculated density (g/cm^3)	4.62	4.29
reliability factors		
R_{wp}	0.0570	0.1267
R_P	0.0424	0.0932
R_I	0.0210	0.0385
R_F	0.0118	0.0187

profiles are presented together with the observed pattern in Figure 3a and the refined structure parameters are summarized in Table 3a.

In contrast to $RbSrNb_2O_6F$, XRD (Figure 2b) and electron diffraction patterns for $LiSrNb_2O_6F$ (Supporting Information) show the reflection conditions of $h + k + l = 2n$, suggesting the $I***$ type space groups ($I4$, $I\bar{4}$, $I4/m$, $I422$, $I4mm$, $I\bar{4}m2$, $I\bar{4}2m$, and $I4/mmm$).[20,21] Among these space groups, we were able to refine the structure successfully based on tetragonal symmetry with the space group of $I4/mmm$ ($a = 3.8304(2)$ Å and $c = 20.837(1)$ Å). A relatively high R factor obtained from Rietveld refinement might be due to the partial collapse of long-range ordering during the ion exchange reaction and a small impurity peak around 28° as shown in Figure 2b. The calculated profiles of $LiSrNb_2O_6F$ are presented in Figure 3b together with the observed pattern. The refined structure parameters and the selected bond lengths are listed in Tables 3b and 4, respectively.

As summarized in Table 4, the Nb−O(1) bond lengths (2.40 Å) for both Rb and Li oxyfluorides are found to be rather longer by ≈0.6 Å than the Nb−O(3) ones (1.74 Å for Rb oxyfluoride and 1.80 Å for the Li one, respectively) as expected from the $Rb(Li)Nb_2O_7$ structure. (The sites of O(1), O(2), and O(3) indicate a central site of two corner-sharing octahedra, an equatorial site, and an apex site of the NbO_6 octahedra in the unit cell, respectively.) Comparing the local structure around Nb in the oxyfluorides with that in their oxide analogues, $ALaNb_2O_7$ (A= Rb and Li), the pronounced difference

(15) Mehring, M. *Principles of High-Resolution NMR in Solids*; Springer-Verlag: Berlin, 1983.
(16) Harris, R. K.; Mann, B. E. *NMR and the Periodic Table*; Academic Press: London, 1978; p 99.
(17) Choy, J. H.; Kim, S. J. *Mol. Cryst. Liq. Cryst.* **1998**, *311*, 429.
(18) Armstrong, A. R.; Anderson, P. A. *Inorg. Chem*, **1994**, *33*, 4366.
(19) Gopalakrishnan, J.; Bhat, V. *Mater. Res. Bull.* **1987**, *22*, 412.; Sato, M.; Abo, J.; Jin, T.; Ohta, M. *J. Alloys Compd.* **1993**, *192*, 81.
(20) Dion, M.; Ganne, M.; Tournoux, M. *Mater. Res. Bull.* **1981**, *16*, 1429.
(21) Debliek, R.; van Lauduyt, J.; Amelinckx, S. *J. Solid State Chem.* **1985**, *59*, 379.

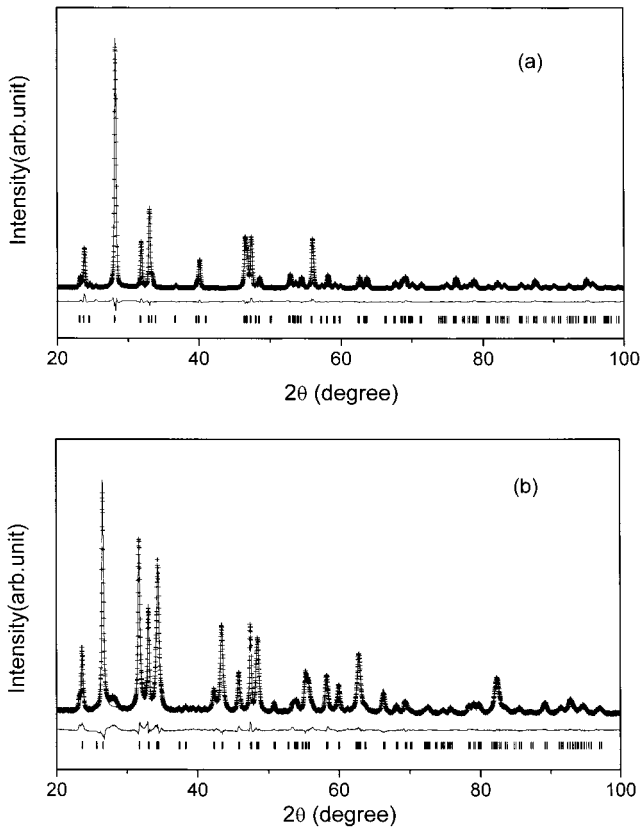

Figure 3. Observed (+) and calculated (−) X-ray diffraction patterns for (a) $RbSrNb_2O_6F$ and (b) $LiSrNb_2O_6F$. Bragg positions and differences are presented below.

Table 3. Atomic Positions and Isotropic Temperature Factors

atom	site	*g*	*x*	*y*	*z*	*B* (Å^2)
			$RbSrNb_2O_6F$			
Rb	1d	0.9[b]	0.5	0.5	0.5	1.0(2)
Sr	1c	1.0	0.5	0.5	0.0	0.8(2)
Nb	2g	1.0	0.0	0.0	0.212(3)	0.5(1)
O(1)/F[a]	1a	1.0	0.0	0.0	0.0	0.7(3)
O(2)/F	4i	1.0	0.0	0.5	0.172(1)	0.7(3)
O(3)	2g	1.0	0.0	0.0	0.367(2)	0.7(3)
			$LiSrNb_2O_6F$			
Li	4d	0.45[b]	0.0	0.5	0.25	2.5(fixed)
Sr	2a	1.0	0.0	0.0	0.0	0.9(5)
Nb	4e	1.0	0.0	0.0	0.385(4)	0.3(3)
O(1)/F	2b	1.0	0.0	0.0	0.5	2.2(8)
O(2)/F	8g	1.0	0.0	0.5	0.095(2)	2.2(8)
O(3)	4e	1.0	0.0	0.0	0.298(3)	2.2(8)

[a] O(1): O_{center} site; O(2): $O_{equatorial}$ site; O(3): O_{apex} site. [b] Site occupancies are fixed as the values obtained by chemical analysis.

between oxyfluorides and oxides is the Nb−O_{center} bond length.[18,19] The Nb−O_{center} (Nb−O(1)) bond lengths for Rb(Li)$SrNb_2O_6F$ are longer than those for $RbLaNb_2O_7$ (2.28 Å) and $LiLaNb_2O_7$ (2.26 Å). However, the Nb−$O_{equatorial}$ and Nb−O_{apex} bonds of oxyfluorides are practically the same as those of oxide analogues.

Na oxyfluoride exists only in hydrated form at ambient conditions because the Na form is rather hygroscopic. Therefore, we obtained powder XRD patterns for the Na form above 200 °C (Figure 2c). However, we were not able to obtain reliable crystallographic data by performing Rietveld refinement due to its reduced intensity and large thermal parameters. From the XRD pattern for the anhydrous Na phase indexed with tetragonal symmetry, the *c*-axis cell parameter (a = 3.848(1) Å; c = 21.796(1) Å) is found to be longer than that for $NaLaNb_2O_7$ (a = 3.904(4) Å; c = 20.99(1) Å), which is also consistent with the result of the Rb and Li phases (Table 2).

Table 4. Selected Bond Distances for $RbSrNb_2O_6F$ and $LiSrNb_2O_6F$ (Å)[a]

$RbSrNb_2O_6F$		$LiSrNb_2O_6F$	
Nb−O(1)/F	2.40(0)	Nb−O(1)/F	2.40(1)
Nb−O(2)/F	1.98(0)	Nb−O(2)/F	1.96(0)
Nb−O(3)	1.74(2)	Nb−O(3)	1.80(6)
Sr−O(1)/F	2.72(0)	Sr−O(1)/F	2.71(0)
Sr−O(2)/F	2.73(0)	Sr−O(2)/F	2.76(3)
O(2)/F−O(3)	2.93(1)	Li−O(2)/F	3.22(0)
O(1)/F−O(2)/F	2.73(0)	Li−O(3)	2.16(3)
O(2)/F−O(2)/F	2.72(0)	Li−Li	2.71(0)
Rb−O(3)	3.11(1)	Li−Nb	3.40(1)
		O(2)/F−O(2)	2.71(0)
		O(1)/F−O(2)	2.76(0)
		O(2)/F−O(3)	2.93(4)

[a] O(1): O_{center} site; O(2): $O_{equatorial}$ site; O(3): O_{apex} site.

Table 5. Lattice Energy Calculated with Respect to Various Anion Distributions in $ASrNb_2O_6F$ (A = Rb and Li)

	distribution of oxygen (O) and fluorine (F)			lattice energy (kJ mol^{-1})
	O_{center} site	$O_{equatorial}$ site	O_{apex} site	
$RbSrNb_2O_6F$	F	4O	2O	4211.904
	O	F/3O	2O	4148.496
	O	4O	F/O	2864.88
$LiSrNb_2O_6F$	F	4O	2O	5253.312
	O	F/3O	2O	5250.064
	O	4O	F/O	3780.144

Fluoride and Oxide Anion Distribution. In the present $ASrNb_2O_6F$ (A = Rb, Na, and Li) oxyfluorides, there are three possible anion sites (O_{center}/$O_{equatorial}$/O_{apex}) for fluorine occupation, as in oxide analogues $ALaNb_2O_7$. At first, we expect that the substituted fluorines are mainly populated at the O_{center} site because of the ionic character of the Nb−O_{center} bond. However, ^{19}F MAS NMR spectra for the present oxyfluorides strongly suggest the presence of fluorine at the $O_{equatorial}$ site (axially asymmetric site in the axial symmetry concept), as will be stated in the subsequent section. Therefore, we attempted to obtain quantitative information on the anion distrubution of O^{2-} and F^- from lattice energy calculation. As shown in Table 5, lattice energies corresponding to three possible fluorine sites were calculated by the MADEL program[14] using Rietveld refinement results. According to the calculation, it is most probable that the fluorine anions are stabilized in the sites of O_{center}(O1) and $O_{equatorial}$(O2). On the other hand, the fluorine occupation of the O_{apex} (O(3)) site is unfavorable compared to the other two sites, which is expected from the covalent character of the Nb−O_{apex} bond (≈1.8 Å). This result is also in good agreement with the F NMR results as discussed in the subsequent section.

In addition to lattice energy calculations, the bond valence sum (BVS) was also calculated for each anion sites according to Brown's formula.[22] The bond valencies of oxide at the O_{center} site are estimated to be 1.32 and 1.34 for Rb and Li compounds, respectively, which are unacceptably low for the divalent oxide ion. In contrast,

(22) Bresse, N. E.; O'Keepe, M. *Acta Crystallogr. B* **1991**, *47*, 192.

when the fluoride ion is placed at the O_{center} site, reasonable values of 1.08 and 1.1 were obtained for Rb and Li compounds, respectively. The O_{center} site (1a and 2b sites for Rb and Li compounds, respectively) can be fully occupied by the substituted fluorine and, therefore, it is evident that ideal anion valency is 1.0.

According to the calculation based on an assumption that the $O_{equatorial}$ site is occupied by oxide, the bond valencies are 2.04 and 2.10 for Rb and Li oxyfluorides, respectively, which agree well with the ideal value of 2.00. When the fluoride is placed at $O_{equatorial}$, the bond valencies are 1.77 and 1.80 for Rb and Li compounds, respectively, which are rather far from the ideal value of 1.00. Therefore, the $O_{equatorial}$ site seems to be occupied by oxide according to BVS calculation. However, it should be taken into account the fact that equivalent crystallographic positions of the $O_{equatorial}$ sites (4i and 8g sites for Rb and Li compounds, respectively) are four and eight in the unit cell, whereas the substituted fluorine amounts are only one and two for Rb and Li compounds, respectively. Therefore, because the Nb−$O_{equatorial}$ bond lengths obtained by structural refinement are the average of Nb−$F_{equatorial}$ and Nb−$O_{equatorial}$ ones, it is thought that the anion valencies for the $O_{equatorial}$ sites, which are calculated from the average bond lengths, should be the averages of oxide and fluoride. According to this assumption, theoretical anion valency is calculated to be 1.75 [$(2.0 \times 3 + 1.0 \times 1)/4$] because only 25% of the $O_{equatorial}$ site is occupied by fluoride. The present BVS calculations for equatorial position provide an ambiguous result on fluorine anion distribution and, therefore, it would be dangerous to expect fluorine position from BVS values because the $O_{equatorial}$ sites are partially populated by fluoride ions.

When fluoride is located at the O_{apex} site (2g and 4e sites for Rb and Li compounds, respectively), the bond valencies are 1.73 and 1.70 for Rb and Li oxyfluorides, respectively, which are rather far from the expected value of 1.50 [$(2.0 \times 1 + 1.0 \times 1)/2$]. On the other hand, the placement of oxide at the O_{apex} site gives reasonable values of 2.00 and 1.99 for Rb and Li compounds, respectively. Therefore, the O_{apex} site is expected to be mainly occupied by oxide, which coincides with the lattice energy calculation result.

^{19}F NMR Analysis. The chemical shift anisotropy (CSA) can be described by three components, δ_{11}, δ_{22}, and δ_{33}, in a principle axis system ($\delta_{11} \geq \delta_{22} \geq \delta_{33}$). The isotropic chemical shift is

$$\delta_i = \frac{1}{3}(\delta_{11} + \delta_{22} + \delta_{33})$$

In the convention by Haeberlen,[23] Mason,[24] and Fyfe,[25]

$$\text{for } |\delta_{11} - \delta_i| \geq |\delta_{33} - \delta_i|, \quad \Delta\delta = \frac{3}{2}(\delta_{11} - \delta_i), \quad \eta = \frac{\delta_{22} - \delta_{33}}{\delta_{11} - \delta_i}$$

$$\text{for } |\delta_{11} - \delta_i| \leq |\delta_{33} - \delta_i|, \quad \Delta\delta = \frac{3}{2}(\delta_{33} - \delta_i), \quad \eta = \frac{\delta_{22} - \delta_{11}}{\delta_{33} - \delta_i}$$

(23) Haeberlen, U. *High-Resolution NMR in Solids-Selective Averaging*; Academic Press: New York, 1976; p 9.
(24) Jameson, C. J.; Mason, J. In *Multinuclear NMR*; Mason, J., Ed.; Plenum Press: New York, 1976; p 7.
(25) Fyfe, C. A. *Solid State NMR for Chemists*; C.F.C. Press: Ontario, 1983; p 119.

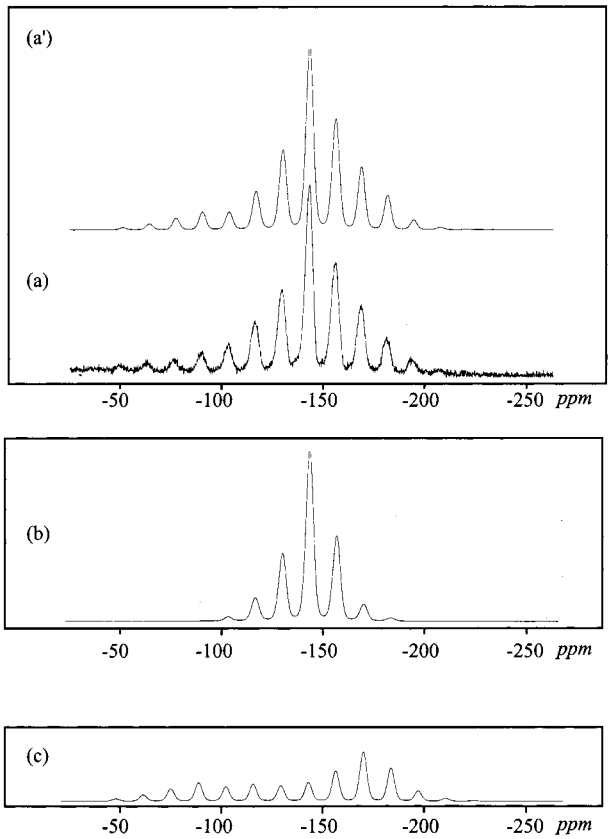

Figure 4. ^{19}F-MAS NMR spectra of $LiSrNb_2O_6F$ with the spinning rate of 5 kHz. (a) Experimental, (a′) simulated, (b) asymmetric site ($\eta = 0.75$), and (c) symmetric site ($\eta = 0.25$).

Thus, in the case of $\delta_{22} = \delta_{33}$ or $\delta_{22} = \delta_{11}$, the value of the asymmetry parameter, η, becomes zero. In other words, if there are at least two symmetry axes, the η value becomes zero and such a system is said to have axial symmetry. In the present system, the O_{center} and O_{apex} sites can be regarded as axially symmetric along the O_{apex}−Nb−O_{center}−Nb−O_{apex} axis in an ideal structure, which results in $\eta \sim 0$, whereas the $O_{equatorial}$ site lacks axial symmetry.

Experimental and theoretical ^{19}F MAS NMR spectra of $LiSrNb_2O_6F$ are shown in Figure 4. The NMR spectra for Rb and Na oxyfluorides are almost the same as those for the Li one (see Supporting Information). The experimental ^{19}F MAS NMR spectra for all the compounds seem to be symmetric, suggesting the presence of the axially asymmetric F-site, that is, $O_{equatorial}$ site. However, assuming that the fluorines are populated only at the $O_{equatorial}$ site (axially asymmetric F-site), the simulated spectra are highly deviated from the experimental ones, especially in the high-order spinning sideband. The shapes of simulated peaks are symmetric and concentrated in the center. On the other hand, the simulations considering two sets of CSA with different axial symmetries made well-fitted profiles, which indicates the presence of two inequivalent F-sites with different chemical environments. As shown in Table 6, the CSA parameters for two fluorine sites (site I and II) are derived from the experimental spectra. One CSA set without axial symmetry has a very symmetric and narrow peak shape (site I), and the other with axial symmetry has an asymmetric and widely spread one (site II).

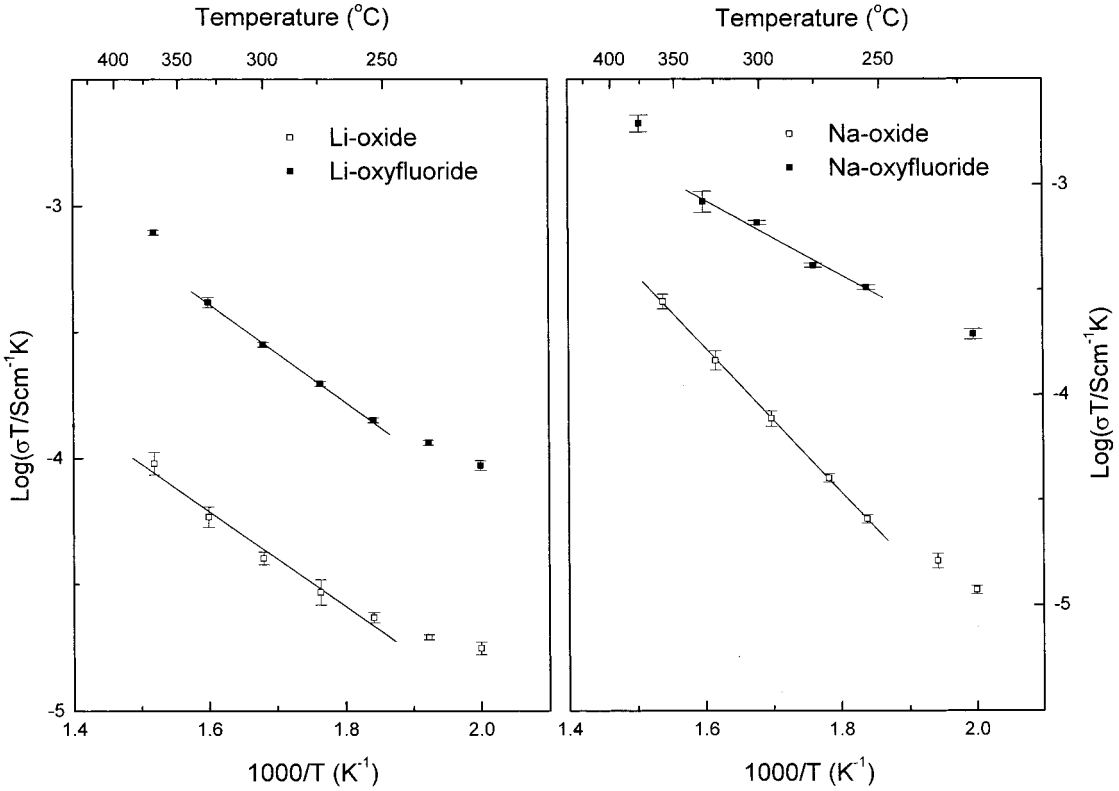

Figure 5. Logarithmic plot of σT as a function of reciprocal temperature for $ASrNb_2O_6F$ and $ALaNb_2O_7$ (A = Li and Na).

Table 6. Chemical Shift Parameters Obtained from ^{19}F-MAS NMR Spectra

	site	δ (ppm)	width	$xG/(1-x)L$[a]	$\Delta\delta$[b]	η[c]
$LiSrNb_2O_6F$	I	−142.59	4.26	0.80	27.89	0.75
	II	−141.94	3.92	0.80	86.33	0.25
$NaSrNb_2O_6F$	I	−144.85	2.87	0.70	27.89	0.80
	II	−143.79	3.42	0.80	78.36	0.30
$RbSrNb_2O_6F$	I	−144.72	2.80	0.85	26.56	0.80
	II	−143.71	3.35	1.00	81.02	0.25

[a] Profile parameter: G, Gaussian line shape; L, Lorentzian line shape. [b] Anisotropy parameter. [c] Asymmetry parameter.

The experimentally determined η values for the site I are far from zero (0.75−0.80 for $ASrNb_2O_6F$, A = Li, Na, and Rb), which excludes the possibility that site I will be the O_{center} or O_{apex} one according to the axial symmetry concept. Therefore, it is reasonable that site I is assigned as the $O_{equatorial}$ site. On the other hand, the η values for site II are 0.25−0.30 for $ASrNb_2O_6F$. Accordingly, site II can be assigned as either the O_{center} or O_{apex} site with axial symmetry. However, from the fact that δ_i values of site II are shifted downfield compared to those of site I for all the compounds, it can be deduced that site II should be the O_{center} one. If the O_{apex} sites are occupied by fluoride ions, the δ_i value for the fluorine (site II) is expected to shift upfield because of the greater overlap of wavefunctions or/and enhanced covalency.[26] Additional evidence can be obtained from the fact that the δ_i values of site II for all the compounds are almost invariant with respect to the different A cations (A = Li, Na, and Rb). If the fluorine is located at the O_{apex} site, the chemical shift should exhibit significant variation with respect to the neighboring A cations because the A−O_{apex} bond lengths as well as the alkali metal coordination around apex oxygen are varied with respect to interlayer cations. However, the experimentally determined chemical shifts (site II) for all the compounds are almost the same, which also supports our assignment. Integration of the two decomposed NMR signals shows that the fluorine ions are statistically distributed over two different sites of each compound (50:50). All these results allow us to conclude that the fluoride ions are stabilized in the $O_{equatorial}$ (axially asymmetric site) and O_{center} (axially symmetric site) sites, which is very consistent with comparable lattice energy values for two anion sites.

Table 7. Activation Energies for $ASrNb_2O_6F$ and $ALaNb_2O_7$ (A = Li and Na)

compounds	activation energy (kJ mol^{-1})	compounds	activation energy (kJ mol^{-1})
$LiSrNb_2O_6F$	37.0	$LiLaNb_2O_7$	46.2
$NaSrNb_2O_6F$	36.9	$NaLaNb_2O_7$	57.2

Ionic Conductivity. The logarithmic ionic conductivities for $ASrNb_2O_6F$ and $ALaNb_2O_7$ (A = Li and Na) are plotted as a function of reciprocal temperature as shown in Figure 5. All the measurements were carried out in a temperature range of 200−400 °C because the present Li oxyfluoride turns into the pyrochlore phase from the perovskite one beyond 400 °C (see Supporting Information). Therefore, we calculated the activation energies of the oxyfluorides in the range of 250−350 °C that exhibits linear correlation well in the Arrhenius plot ($\log(\sigma T)$ vs $1/T$) (Table 7).

Here, we have compared the Li^+ and Na^+ ionic conductivities of the oxyfluorides with those of the corresponding oxides to probe the effect of fluorine substitution and found that the former ones are larger than the latter ones by ≈1 order of magnitude. Such enhanced conductivity suggests that the substitution of

(26) Turner, G. L.; Chung, S. E.; Oldfield, E. *J. Magn. Reson.* **1985**, *64*, 316.

less polarizable fluorine for oxygen is beneficial to Li and Na ion mobility in the interlayer space. When the fluoride ion occupies the equatorial and central oxygen sites surrounding niobium, it is expected that the net charge of O^{2-}(apex) will be reduced because the Nb−O(apex) bond becomes more covalent because of the weakening of Nb−O(equatorial) and Nb−O(center) upon fluorine substitution. This effect tends to decrease the potential barrier and to increase the mobility of Li^+ and Na^+ cations. However, if a significant amount of fluorines are populated at the O_{apex} site, the ionic conductivity should decrease because of the smaller polarizability of fluorine (hard base). Activation energies derived from an Arrhenius plot also support the present explanation that the fluorine substitution reduces the activation barrier to Li^+ and Na^+ mobility. As listed in Table 7, the activation energies for Na and Li oxyfluorides are slightly smaller than those for the corresponding oxides, respectively.

Conclusion

In an attempt to study the fluorine substitution effect on ionic conductivity, a new series of layered perovskite oxyfluorides, $ASrNb_2O_6F$ (A = Li, Na, and Rb), has been synthesized and analyzed by the X-ray diffraction method, ^{19}F MAS NMR spectroscopy, and impedance spectroscopy. Powder X-ray diffraction patterns show that the crystal structures of the oxyfluorides are analogous to those of the corresponding La niobates, $ALaNb_2O_7$ (A = Li, Na, and Rb). The spatial distribution of fluorine anions in Nb octahedra in the perovskite slab is systematically studied by ^{19}F MAS NMR analysis and lattice energy calculation. The NMR peak simulation allows us to conclude that the fluorine anions prefer to occupy two inequivalent sites, the O_{center} site (the central site of two corner-sharing NbO_6 octahedra) and the $O_{equatorial}$ site (the equatorial site), but avoid the O_{apex} site (the apex site of NbO_6 octahedra), which was also confirmed by lattice energy calculations. Finally, we have compared the ionic conductivities for the oxyfluorides with those for the corresponding oxides to study the effect of fluorine doping. As a result, it becomes evident that the interlayer cationic conductivity is enhanced because of a weakening of bond strength between the alkali metal and oxygen.

Acknowledgment. This work is financially supported by the Korea Research Foundation (1997-011-D0019). The authors also wish to acknowledge the fellowships by the Ministry of Education (Brain Korea 21 program) and Ministry of Science and Technology (National Research Laboratory 1999).

Supporting Information Available: Figures of [001] zone axis electron diffraction patterns and temperature-dependent XRD patterns for $LiSrNb_2O_6F$ and $RbSrNb_2O_6F$; ^{19}F MAS NMR spectra of $NaSrNb_2O_6F$ and $RbSrNb_2O_6F$ with the spinning rate of 5 kHz (PDF). This material is available free of charge via the Internet at http://pubs.acs.org.

CM000673G